Applied Catalysis B: Environmental 127 (2012) 227–233

Contents lists available at SciVerse ScienceDirect

Applied Catalysis B: Environmental

journal homepage: www.elsevier.com/locate/apcatb

Photocatalytic activity of titania layer prepared by oxidizing titanium compounds on titanium plate surface

Hiromasa Nishikiori[a,*], Masato Takei[a], Kyoichi Oki[b], Syouta Takano[a], Nobuaki Tanaka[a], Tsuneo Fujii[c]

[a] Department of Environmental Science and Technology, Faculty of Engineering, Shinshu University, 4-17-1 Wakasato, Nagano 380-8553, Japan
[b] Miyama Co., Ltd, 1-1-12 Tanbajima, Nagano 381-2283, Japan
[c] Nagano Prefectural Institute of Technology, 813-8 Shimonogo, Ueda, Nagano 386-1211, Japan

ARTICLE INFO

Article history:
Received 10 June 2012
Received in revised form 22 August 2012
Accepted 26 August 2012
Available online 31 August 2012

Keywords:
Titania
Photocatalysis
Oxidation
Titanium nitride
Carbon-doped titanium nitride

ABSTRACT

Anatase-type nanocrystalline titania layers were prepared by oxidizing the crystalline titanium nitride and carbon-doped titanium nitride phases prepared on a titanium plate surface. Identification of the crystalline phase was confirmed by the XRD patterns and Raman spectra of these plates. The photocatalytic activity of the plates was evaluated by observing the photocatalytic degradation process of acetaldehyde gas during UV irradiation by gas chromatography. A relatively larger amount of the anatase phase was formed on the very thin surface layer by heating the carbon-doped titanium nitride phase at 500 °C, and it exhibited a higher photocatalytic activity for the acetaldehyde degradation. The activity was determined not only by the amount of the anatase phase, but also by the crystallite size depending on the surface area and charge transfer efficiency. The photocatalytic activity is suggested to be due to the anatase phase existing on the thin surface layer accessible to the reactants.

1. Introduction

Titania photocatalyst films on metal plates are useful as photovoltaic electrodes for solar cells [1–3] or water splitting systems [4–7]. For example, titania-coated metal plates can induce hydrogen and oxygen on the metal and titania side surfaces, respectively, in water during UV irradiation [6]. This is an effective way to separate the hydrogen and oxygen gases even though it is difficult for such a reaction using photocatalytic power. Titania films are formed on the surface of titanium plates due to their oxidation, e.g., by anodic oxidation [8–10]. The oxidative heating method as a simpler and easier method was developed for economic and ecological advantages. However, it is difficult to obtain nanocrystalline titania crystals having a high photocatalytic activity because an inactive amorphous titania phase film is formed on the titanium plate surface by heating [11,12]. Control of the crystal structure on the titanium surface is required to form the highly active anatase phase. The atatase phase can be formed by oxidizing titanium nitride, titanium carbide, and titanium disulfide [13–16], i.e., the substitution of nitrogen, carbon, and sulfur by oxygen. Titanium carbonitride is harder and more oxidation resistant than titanium nitride [17,18]. Titanium nitride can be doped with carbon in order to control the phase transition during the oxidative heating. Titanium nitride and the carbon-doped titanium nitride phase are easily prepared by the sputtering or arc ion plating of titanium under the appropriate reactive gas atmospheres [19,20].

In this study, we tried to prepare the nanocrystalline anatase layer by oxidation of the titanium nitride and carbon-doped titanium nitride phase on titanium plates. Practically, the amorphous TiO_2, amorphous and crystalline TiN, and carbon-doped TiN phases on the titanium plate surface were heated at various temperatures in air. The structure of the surface layer was characterized by XRD analysis and Raman spectroscopy, and then its photocatalytic activity was examined by acetaldehyde degradation in order to clarify the phase transition mechanism and photoactive condition of the phase.

2. Experimental

2.1. Materials

The titanium plates (plate Ti) were purchased from Takeuchi Kinzoku-Hakufun Kogyo Co., Ltd. The amorphous titanium nitride phase, formed on the Ti plate surface by glow discharge in an ammonia and nitrogen gas atmosphare (TiN-a plate), was obtained from Hokunetsu Co., Ltd. The crystalline titanium nitride and carbon-doped titanium nitride phases, formed on a Ti plate by arc discharge in nitrogen (TiN-c plate) and methane + nitrogen (TiCN plate) gas atmospheres, respectively, were also obtained from Hokunetsu Co., Ltd. The C/N atomic ratio was 0.5. These plates were

* Corresponding author. Tel.: +81 26 269 5536; fax: +81 26 269 5550.
E-mail address: nishiki@shinshu-u.ac.jp (H. Nishikiori).

0926-3373/$ – see front matter © 2012 Elsevier B.V. All rights reserved.
http://dx.doi.org/10.1016/j.apcatb.2012.08.023

heated at 450 °C for 20 h, and then at 500–600 °C for 20 h. The TiCN plate was also heated at 400 °C for 20 h. The heating was performed using a tubular heater in the air (ISUZU EPKRO-11K).

Powder samples of the anatase- and rutile-type titanias were perchased from Kanto Chemical Co., Inc., for use as the standerd samples for the Raman analysis. Acetaldehyde was purchased from Wako Pure Chemical Industries, Ltd., and used for the photocatalytic degradation without further purification. The dry air gas (ca. 79% nitrogen + 21% oxygen) was obtained from Okayasanso Co., Ltd.

2.2. Measurements

The XRD patterns and Raman spectra of these plates were obtained in order to identify their crystalline phase. The XRD analysis was conducted using an X-ray diffractometer (Rigaku RINT2000) with CuKα radiation. The crystal structure was determined using the inorganic crystal structure database of The Crystallographic Society of Japan. The size of the titania crystallites of each sample was estimated from its full-width at half-maximum of the 25.3° peak for anatase and the 27.4° peak for rutile in the XRD pattern using Sherrer's equation, $D = 0.9\lambda/\beta\cos\theta$. The Raman spectra were obtained using a laser Raman spectrophotometer (JASCO NRS-3100) by 532 nm laser irradiation. UV–vis diffuse reflectance spectra were observed using a UV–vis–near IR spectrophotometer (Shimadzu UV-3150). The surface morphology of the plates was observed using a field emission scanning electron microscope (Hitachi S-4100). The surface morphology and elemental mapping of the plates were obtained using a field emission scanning electron microscope (JEOL JSM-7000F).

Each sample plate (5 cm × 2 cm) was immersed in 10 cm^3 of an MB aqueous solution (2.0×10^{-5} mol dm^{-3}) for 12 h. It was confirmed that the adsorption of MB was equilibrated. The amount of the MB adsorbed on each plate was estimated from the equilibrium concentration in the MB aqueous solution using the UV–vis–near IR spectrophotometer.

The photocatalytic activities of the sample plates were examined by photocatalytic degradation of the acetaldehyde gas during UV irradiation, which was conducted using a 4 W black light bulb (TOSHIBA FL4BLB). The plates were first irradiated by UV light for 24 h in order to degrade the adsorbed organic substances. Each plate (1 cm × 1 cm) was placed in a glass vial. Acetaldehyde gas diluted with dry air was injected into the the vial in which its concentration was 84 ppmv. The vial was kept at ambient temperature in the dark for 1 h until the acetaldehyde adsorption had equilibrated. The degradation process of acetaldehyde was observed during the UV irradiation using a gas chromatograph (HNU systems GC-311).

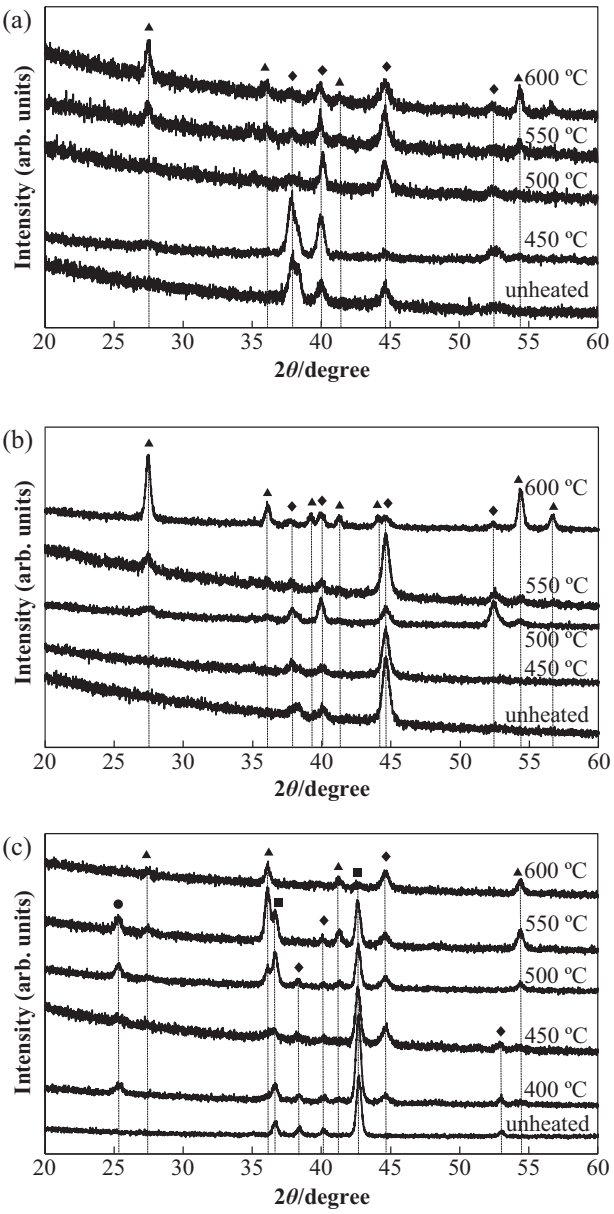

Fig. 1. XRD patterns of (a) Ti plate, (b) TiN-a plate, and (c) TiN-c plate unheated and heated at 400–600 °C. The peaks were assigned to the (♦) Ti metal, (■) rock salt structure of TiN, (●) anatase TiO_2, and (▲) rutile TiO_2.

3. Results and discussion

3.1. Formation of titania by oxidizing titanium nitride phase

Fig. 1 shows the XRD patterns of the Ti, TiN-a, and TiN-c plates unheated and heated at 400–600 °C. The XRD patterns of the Ti and TiN-a plates exhibited peaks at 38.4°, 40.2°, 44.6°, and 53.0° assigned to the (0 0 2), (1 0 1), (2 0 0), and (1 0 2) planes of the titanium metal, respectively. The titanium substrate under the amorphous TiN layer was observed in the pattern of the TiN-a plate. The rutile titania phase exhibiting the peaks for the (1 1 0), (1 0 1), (1 1 1), and (2 1 1) planes at 27.4°, 36.1°, 41.2°, and 54.3°, respectively, was formed in the Ti and TiN-a plates heated at 550 °C and higher. The XRD pattern of the unheated TiN-c plate exhibited strong peaks at 36.6° and 42.6°, which were assigned to the (1 1 1) and (2 0 0) planes of the rock salt structure of the TiN phase, respectively, in addition to the peaks due to the titanium substrate. In the pattern for the TiN-c plate even heated at 400 °C, a peak was seen at around 25.3° assigned to the (1 0 1) plane of the anatase titania. In addition, the rutile phase was observed in the TiN-c plate heated at 550 °C and higher. The anatase phase was almost completely transformed into the rutile phase at 600 °C.

The crystalline TiN phase was transformed into the anatase titania phase because they have similar structures. Titania consists of octahedral TiO_6 units. The rock salt structure is made by stacking the octahedral units without any spaces, which has an excess number of titanium atoms over the stoichiometric TiO_2. The anatase structure contains half the number of titanium atoms. The anatase structure is formed by substitution of the two nitrogen atoms of the rock salt TiN with one oxygen atom during the oxidative heating.

Fig. 2 shows the Raman spectra of the Ti, TiN-a, and TiN-c plates unheated and heated at 400–600 °C compared to those of the anatase and rutile titania. The anatase titania exhibited peaks at 141, 391, 512, and 634 cm^{-1} [21–23]. The rutile titania exhibited peaks at 239, 445, and 608 cm^{-1} [23]. For the Ti and TiN-a plates, broad peaks were observed at around 200–400 and 600 cm^{-1},

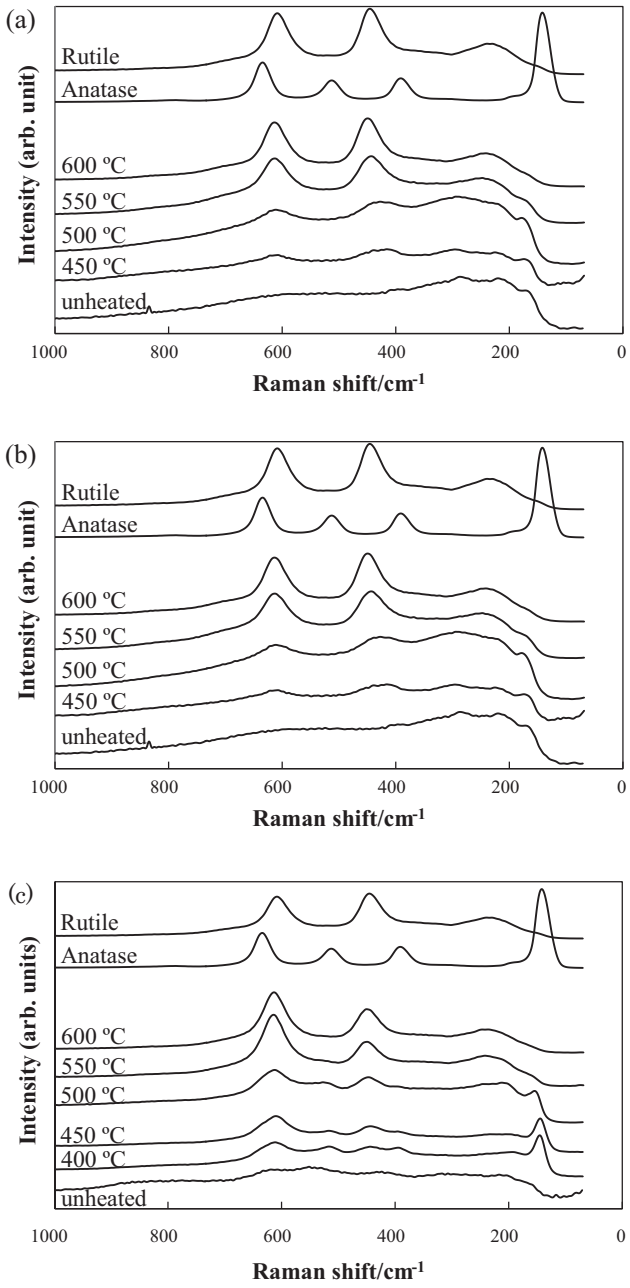

Fig. 2. Raman spectra of (a) Ti plate, (b) TiN-a plate, and (c) TiN-c plate unheated and heated at 400–600 °C.

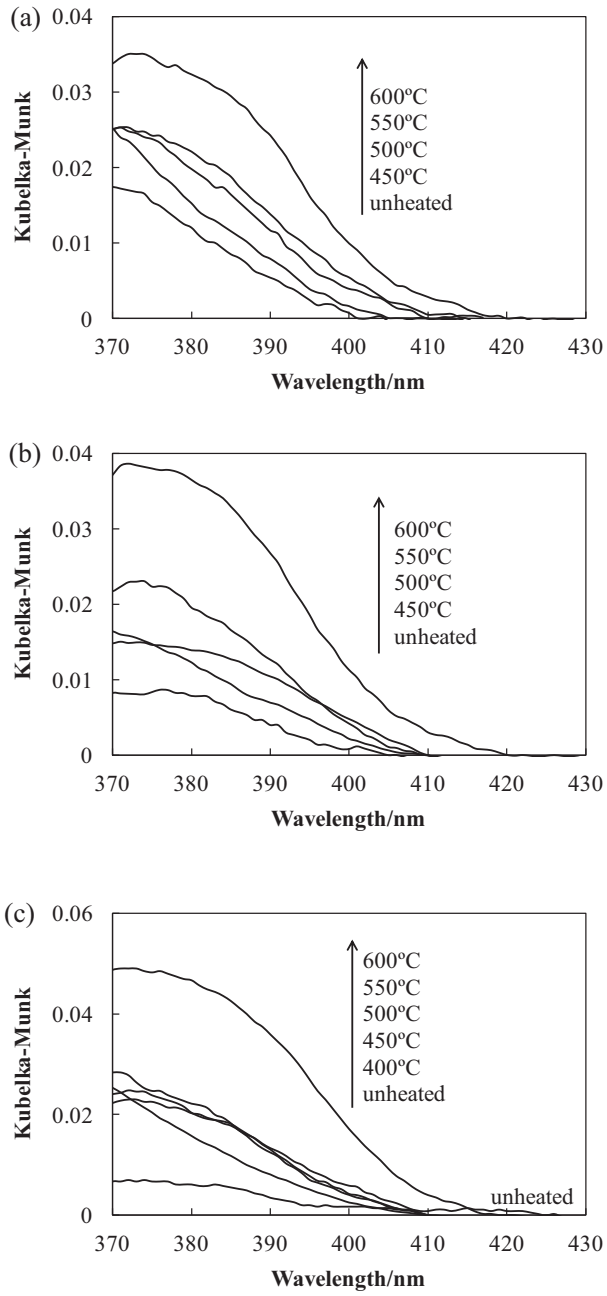

Fig. 3. UV–vis diffuse reflectance spectra of (a) Ti plate, (b) TiN-a plate, and (c) TiN-c plate unheated and heated at 400–600 °C.

which can be assigned to the amorphous titania formed on the plate surface [24–26]. The rutile peaks clearly appeared in the spectra of these plates after heating and their relative intensity increased with an increase in the temperature. The Raman spectra reflect the very shallow surface of the plates. These results indicated that a very thin rutile phase was formed on the surface even at 450 °C although the rutile phase was observed at 550 °C and higher in the XRD patterns. The anatase titania phase was not formed from the amorphous titania phase because the anatase phase was quickly transformed into the rutile phase. The amorphous titania formed on the titanium surface should contain a large number of oxygen vacancies. The oxygen vacancies promote cleavage of the TiO bonds in the anatase structure which reduces the lattice volume and forms the denser rutile structure [26,27].

The broad peaks observed at 227, 314, and 560 cm^{-1} in the unheated TiN-c plate are due to the rock salt structure of TiN [28]. The anatase peaks were observed in the plates heated at 400 and 450 °C. The rutile peak intensity also increased with an increase in the temperature. The anatase peaks almost completely disappeared at temperatures higher than 500 °C. Raman spectroscopy can probe the structure of the thin surface layer because the laser light is scattered by several tens of nanometer-sized particles depending on their size and density. The very thin layer on the plate surface consisted of the rutile phase although the thick anatase phase remained under the layer based on the XRD patterns. Oxidation gradually occurred from the surface of the plate in the air.

Fig. 3 shows the UV–vis diffuse reflectance spectra of the Ti, TiN-a, and TiN-c plates unheated and heated at 400–600 °C. The ordinate indicates the Kubelka–Munk function approximating the absorbance. The absorption edges were observed at around 400 nm

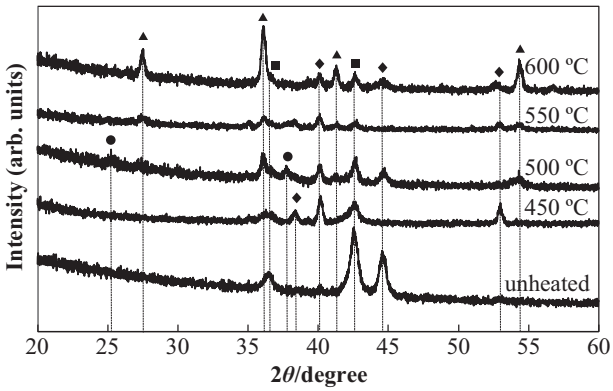

Fig. 4. XRD patterns of TiCN plate unheated and heated at 450–600 °C. The peaks were assigned to the (♦) Ti metal, (■) rock salt structure of TiN, (●) anatase TiO_2, and (▲) rutile TiO_2.

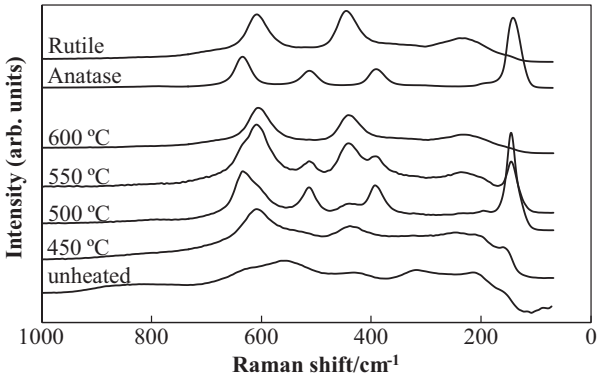

Fig. 5. Raman spectra of TiCN plate unheated and heated at 450–600 °C.

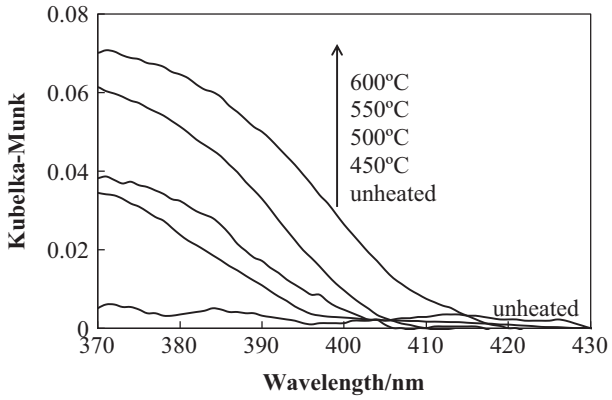

Fig. 6. UV–vis diffuse reflectance spectra of TiCN plate unheated and heated at 450–600 °C.

in the unheated Ti and TiN-a plates containing the amorphous titania phase on the surface because its band gap energy was close to that of the anatase titania [29,30]. The absorbance increased and the band edge was red-shifted with an increase in the temperature. The absorption edge approached that of rutile titania, ca. 420 nm. On the other hand, the weak absorption band and the absorption edge at a longer wavelength, ca. 425 nm, were observed in the untreated TiN-c plate because it contained the crystalline TiN phase [13]. The visible absorption band disappeared at 400 °C due to the anatase titania formation. The red shift of the absorption edge was also observed by heating at a higher temperature due to the rutile phase formation.

3.2. Influence of doping with carbon on titania formation

Titanium nitride was doped with carbon in order to control the phase transition during oxidative heating because carbon-doped

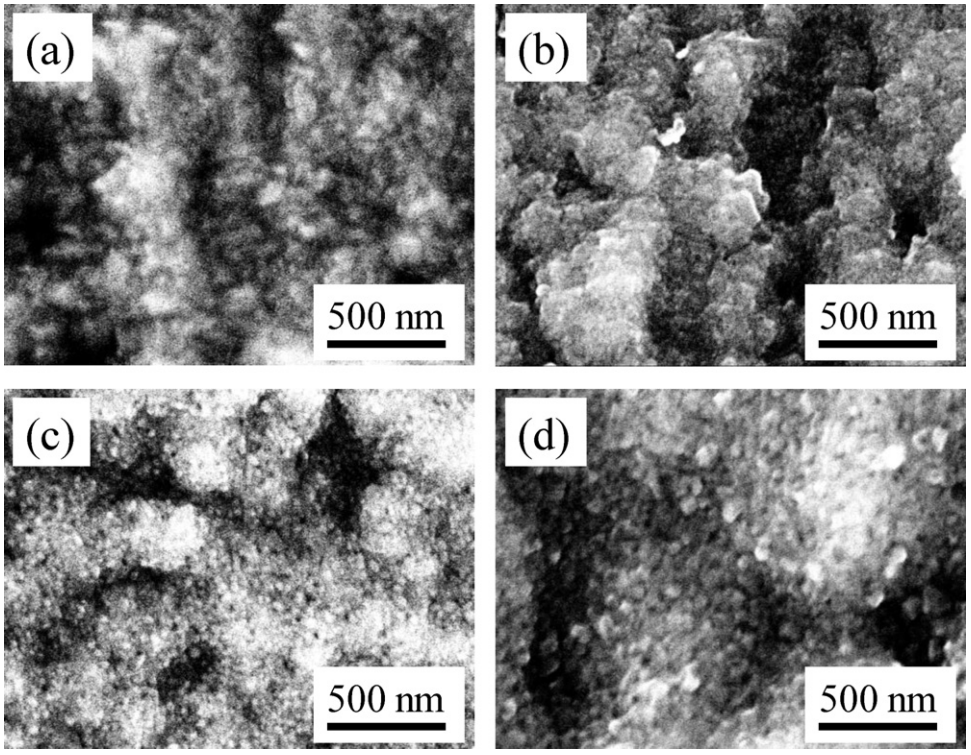

Fig. 7. SEM images of TiCN plate (a) unheated and heated at (b) 450, (c) 500, and (d) 600 °C.

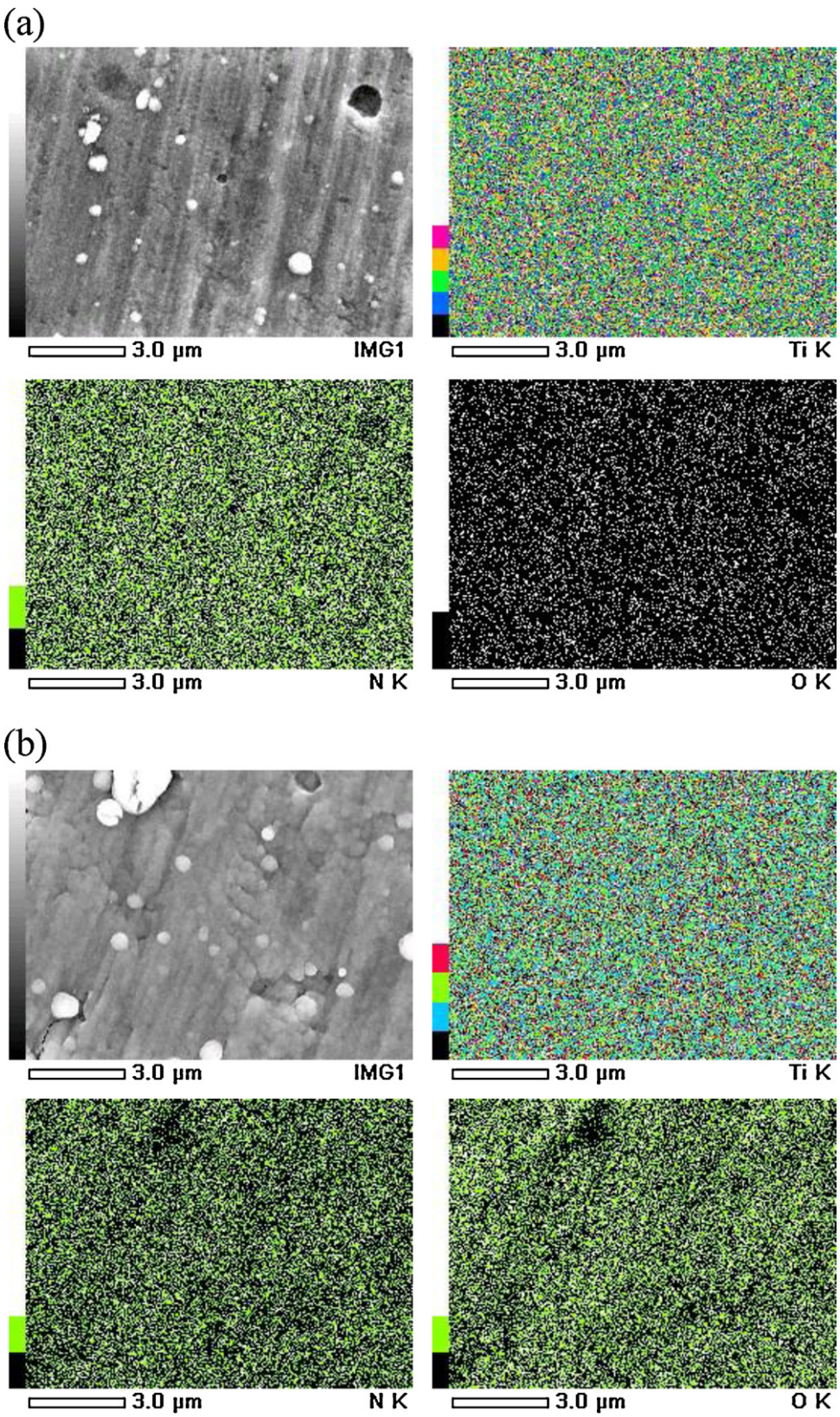

Fig. 8. SEM images and EDX elemental mapping of TiCN plate (a) unheated and (b) heated at 500 °C.

titanium nitride is harder to be oxidized than titanium nitride. Figs. 4 and 5 show the XRD patterns and Raman spectra of the TiCN plates unheated and heated at 450–600 °C. Table 1 shows the crystallite sizes of the titania in the heated plates estimated by the XRD analysis.

The XRD pattern of the unheated TiCN plate exhibited strong peaks assigned to the (1 1 1) and (2 0 0) planes of the rock salt structure of the TiN phase in addition to the peaks due to the titanium foundation. The carbon doping did not change the TiN crystal structure because titanium nitride and titanium carbide have the same

Table 1
Crystallite sizes (/nm) of the titania in the Ti, TiN-a, TiN-c, and TiCN plates heated at 400–600 °C estimated by an XRD analysis.

Temperature (°C)	Ti		TiN-a		TiN-c		TiCN	
	Anatase	Rutile	Anatase	Rutile	Anatase	Rutile	Anatase	Rutile
400					6.8 ± 0.6	–		
450	–	–	–	–	10.7 ± 1.8	–	–	–
500	–	–	–	9.7 ± 1.5	9.9 ± 1.5	9.6 ± 1.4	11.2 ± 1.8	9.9 ± 1.6
550	–	11.1 ± 1.6	–	9.7 ± 1.5	10.5 ± 1.7	18.5 ± 1.5	–	15.7 ± 1.9
600	–	11.1 ± 1.7	–	21.2 ± 2.5	–	14.1 ± 2.0	–	22.2 ± 2.8

structure. The anatase phase was formed by heating at 500 °C as identified by the small peak at around 25.3°. The rutile phase was observed by heating at 550 °C and higher temperatures. The anatase phase was almost completely transformed into the rutile phase at 550 °C. The phase transition into anatase occurred at a higher temperature than for the TiN-c plate.

The rock salt structure of TiN was observed in the Raman spectrum of the unheated plate similar to that of the TiN-c plate. The anatase peaks were observed in the plates heated at 500 and 550 °C. The anatase and rutile peaks were seen in the plate heated at 550 °C even though the anatase phase was not observed in the XRD pattern. This indicated that the anatase phase remained on the thin surface layer. The anatase peaks almost completely disappeared at 600 °C. A greater amount of the anatase phase was observed in the TiCN plate heated at a higher temperature than in the TiN-c plate because the phase transition into anatase and rutile on the surface occurred at a higher temperature than for the TiN-c plate.

Fig. 6 shows the UV–vis diffuse reflectance spectra of the TiCN plate unheated and heated at 450–600 °C. The TiCN plate exhibited the weak and broad absorption band over 370 – 430 nm because it contained the C-doped crystalline TiN phase with a mirror plane [13,15]. The visible absorption band disappeared and the UV band intensity increased at 450 °C due to the anatase titania formation. The red shift of the absorption edge was also observed by heating at a higher temperature due to the rutile phase formation.

Fig. 7 shows the SEM images of the TiCN plates unheated and heated at 450–600 °C. Small particles of carbon-doped titanium nitride were observed in the images of the unheated plate and one heated at 450 °C. The particles size is smaller than 50 nm. Further smaller particles were formed after heating at 500 °C, which are titania particles. Growth of these particles occurred by heating at 600 °C.

Fig. 8 shows the EDX elemental mapping of the plates unheated and heated at 500 °C. The relative amounts of nitrogen and carbon decreased by the heating, whereas that of oxygen clearly increased. Oxidative heating induced the titania formation by substituting nitrogen and carbon by oxygen on the carbon-doped titania nitride surface.

3.3. Photocatalytic activity

Photocalytic degradation of acetaldehyde gas during UV irradiation was observed by gas chromatography. The amount of acetaldehyde adsorbed on the sample plates was too low to be estimated by gas chromatography because the surface layer was very thin and the total surface area of the films was very small. The amount of the methylene blue adsorbed on each plate is summarized in Table 2. The adsorption capacity of the plates tended to decrease with an increase in their crystallite size shown in Table 1. The adsorption capacity of the plates heated at 600 °C was especially low due to their small surface area.

Fig. 9 shows the changes in the relative concentration of acetaldehyde during UV irradiation in the presence of the Ti, TiN-a, TiN-c, and TiCN plates heated at 500 °C. The concentration gradually decreased with an increase in the irradiation time using each plate. About 25–30% of the acetaldeyde degraded during the 24-h irradiation using the Ti, TiN-a, and TiN-c plates, indicating that their activities were close and slightly dependent on their crystal phase. The Ti and TiN-a plates consist of amorphous and rutile phases. The TiN-c plate having the anatase phase on the surface seems the most active of these plates although the titania crystallite sizes and adsorption capacities for the three plates are almost the same as shown in Tables 1 and 2. On the other hand, the TiCN plate degraded 60% of the acetaldehyde during the 24-h irradiation. The crystallite sizes of the anatase and rutile and the adsorption capacity for this plate are not very different from those of the other plates. The active anatase-type titania phase was formed on the surface of the carbon-doped titanium nitride plate. The highest relative amount of the anatase phase was clearly found in the TiCN plate of all the plates based on the Raman spectra. The photocatalytic activity is suggested to be due to the anatase phase presence on the thin surface layer accessible to the reactants.

Table 2
Methylene blue adsorption amount (/10^{-9} mol cm^{-2}) of the Ti, TiN-a, TiN-c, and TiCN plates heated at 400–600 °C.

Temperature (°C)	Ti	TiN-a	TiN-c	TiCN
400			2.2 ± 1.0	
450	1.2 ± 0.8	1.5 ± 1.0	2.5 ± 0.8	1.6 ± 0.5
500	1.0 ± 0.6	2.1 ± 1.0	1.5 ± 0.7	1.4 ± 0.6
550	1.1 ± 0.4	1.1 ± 0.5	1.0 ± 0.5	1.0 ± 0.5
600	1.0 ± 0.7	0.3 ± 0.2	1.0 ± 0.7	0.2 ± 0.1

Fig. 10 shows the change in the relative acetaldehyde concentration during UV irradiation in the presence of the TiCN plates heated at 450–600 °C. The concentration gradually decreased with an increase in the irradiation time using each plate. The degradation rate was faster in the order of the plates heated at 500, 450, 550, and 600 °C. The activity of the plate heated at 550 °C was clearly lower than that of the plate heated at 450 °C even though a higher amount of the anatase phase was formed on the surface of the plate heated at 550 °C. The plate heated at 550 °C consisted of relatively large rutile particles, whose crystallite size was 15.7 nm. Also, its

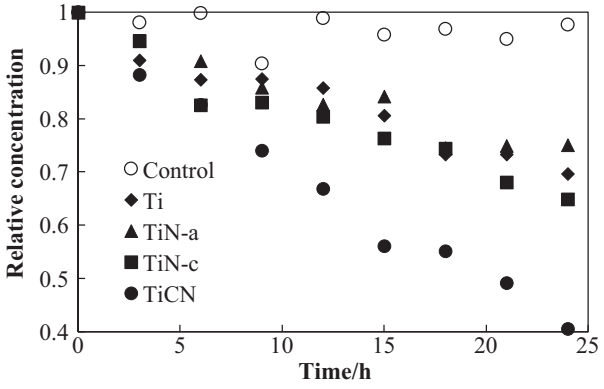

Fig. 9. Change in acetaldehyde concentration during UV irradiation in the presence of Ti plate, TiN-a plate, TiN-c plate, and TiCN plate heated at 500 °C.

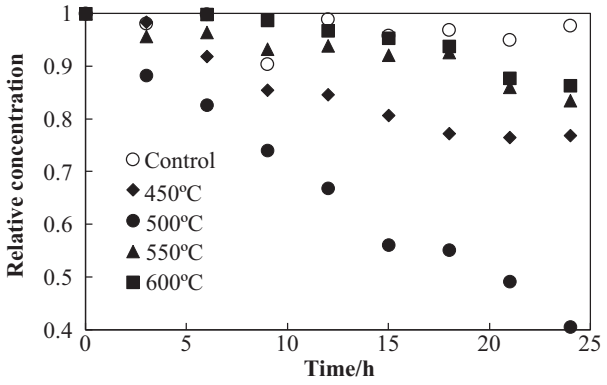

Fig. 10. Change in acetaldehyde concentration during UV irradiation in the presence of TiCN plate heated at 450–600 °C.

adsorption capacity was lower than those of the plates heated at 450 and 550 °C. These results indicated that the activity was determined by the balance of the amount of the anatase phase and the crystallite size depending on the surface area and charge transfer efficiency [31].

4. Conclusions

The phases of amorphous TiO_2, amorphous and crystalline TiNs, and carbon-doped TiN on the Ti plate surface were oxidized by heating at various temperatures. The structure of the surface layer was characterized by an XRD analysis and Raman spectroscopy, and then its photocatalytic activity was determined by acetaldehyde degradation in order to clarify the phase transition mechanism and photoactive condition of the phase. The rutile-type nanocrystalline titania layer was formed by oxidizing the amorphous TiO_2 phase and amorphous and crystalline TiN phases. An anatase-type nanocrystalline titania layer was prepared from the crystalline TiN and carbon-doped TiN phases due to their structural similarities. The anatase phase was transformed into the rutile phase by heating at a higher temperature. Carbon doping inhibited the phase transition. Consequently, the relatively highest amount of the anatase phase was formed on the very thin surface layer by heating the carbon-doped TiN phase at 500 °C and it exhibited the highest photocatalytic activity for acetaldehyde degradation. This activity was based not only on the amount of the anatase phase, but also on the crystallite size depending on the surface area and charge transfer efficiency. The photocatalytic activity is suggested to be due to the anatase phase present on the thin surface layer accessible to the reactants.

References

[1] B. O'Regan, M. Grätzel, Nature 353 (1991) 737–740.
[2] M.K. Nazeeruddin, A. Kay, I. Rodicio, R. Hamphry-Baker, E. Müeller, P. Liska, N. Vlachopoulos, M. Grätzel, Journal of the American Chemical Society 115 (1993) 6382–6390.
[3] M. Grätzel, Journal of Photochemistry and Photobiology C: Photochemistry Review 4 (2003) 145–153.
[4] A. Fujishima, K. Honda, Nature 238 (1972) 37–38.
[5] K. Maeda, K. Teramura, D. Lu, T. Takata, N. Saito, Y. Inoue, K. Domen, Nature 440 (2006) 295.
[6] M. Kitano, M. Takeuchi, M. Matsuoka, J.A. Thomas, M. Anpo, Catalysis Today 120 (2007) 133–138.
[7] A. Kudo, Y. Miseki, Chemical Society Reviews 38 (2009) 253–278.
[8] K.J. Hartig, N. Getoff, International Journal of Hydrogen Energy 11 (1986) 773–781.
[9] H. Habazaki, M. Uozumi, H. Konno, K. Shimizu, P. Skeldon, G.E. Thompson, Corrosion Science 45 (2003) 2063–2073.
[10] S. Takeda, S. Suzuki, H. Odaka, H. Hosono, Thin Solid Films 392 (2001) 338–344.
[11] G. Rådegran, J. Lausmaa, L. Mattsson, U. Rolander, B. Kasemo, Journal of Electron Microscopy Technique 19 (1991) 99–106.
[12] E. Charles, H. Sykes, M.S. Tikhov, R.M. Lambert, Journal of Physical Chemistry B 106 (2002) 7290–7294.
[13] T. Morikawa, R. Asahi, T. Ohwaki, K. Aoki, Y. Taga, Japanese Journal of Applied Physics 40 (2001) L561–L563.
[14] Y. Choi, T. Umebayashi, S. Yamamoto, S. Tanaka, Journal of Materials Science Letters 22 (2003) 1209–1211.
[15] M. Shen, Z. Wu, H. Huang, Y. Du, Z. Zou, P. Yang, Materials Letters 60 (2006) 693–697.
[16] T. Umebayashi, T. Yamani, H. Itoh, K. Asai, Applied Physics Letters 81 (2002) 454–456.
[17] W. Lengauer, in: R. Riedel (Ed.), Handbook of Ceramic Hard Materials, Wiley-VCH, Weinheim, 2000, pp. 202–252.
[18] J.H. Hsieh, C. Li, W. Wu, A.L.K. Tan, Journal of Materials Processing Technology 140 (2003) 662–667.
[19] C.V. Cooper, R.A. Wagner, Thin Solid Films 197 (1991) 293–302.
[20] Y. Zhao, G. Lin, J. Xiao, W. Lang, C. Dong, J. Gong, C. Sun, Applied Surface Science 257 (2011) 5694–5697.
[21] T. Ohsaka, F. Izumi, Y. Fujiki, Journal of Raman Spectroscopy 7 (1978) 321–324.
[22] H. Berber, H. Tang, F. Lévy, Journal of Crystal Growth 130 (1993) 108–112.
[23] U. Balachandran, N.G. Eror, Journal of Solid State Chemistry 42 (1982) 276–282.
[24] P.J. Huang, H. Chang, C.T. Yeh, C.W. Tsai, Thermochimica Acta 297 (1997) 85–92.
[25] A. Niilisk, M. Moppel, M. Pärs, I. Sildos, T. Jantson, T. Avarmaa, R. Jaaniso, J. Aarik, Central European Journal of Physics 4 (2006) 105–116.
[26] F.D. Hardcastle, H. Ishihara, R. Sharma, A.S. Biris, Journal of Materials Chemistry 21 (2011) 6337–6345.
[27] R.D. Shannon, J.A. Pask, Journal of the American Ceramic Society 48 (1965) 391–398.
[28] L. Escobar-Alarcon, V. Medina, E. Camps, S. Romero, M. Fernandez, D. Solis-Casados, Applied Surface Science 257 (2011) 9033–9037.
[29] M. Zhang, G. Lin, C.g. Dong, L. Wen, Surface and Coatings Technology 201 (2007) 7252–7258.
[30] M. Takayanagi, Y. Imai, K. Tajima, Chemistry Letters 36 (2007) 876–877.
[31] B. Ohtani, O.O.P. Mahaney, F. Amano, N. Murakami, R. Abe, Journal of Advanced Oxidation Technologies 13 (2010) 247–261.